2022 IEEE-RAS 21th International Conference on Humanoid Robots (Humanoids)
November 28-30, 2022. Ginowan, Japan.

Humanoid Running based on 3D COG-ZMP Model and Resolved Centroidal Viscoelasticity Control

Zewen He and Ko Yamamoto

***Abstract*— Dynamic motion including a flight phase is a challenging topic in humanoid robotics research, especially a running motion. The stability in the stance phase and the accuracy of the foot control in flight phase are important for this kind of motion. This paper presents a humanoid running motion, applying the resolved viscoelasticity control (RVC) including the centroidal viscoelasticity that we proposed in the previous report. Combining the RVC with real-time trajectory modification, we can achieve a stable foot landing and eventually stable running motion. Effectiveness of this control approach is validated by forward dynamics simulations.**

I. Introduction

The motion control theories for the biped locomotion of a humanoid robot have been investigated in the last few decades. Although Boston Dynamics released some videos in which a humanoid ATLAS demonstrated hopping, running and parkour motions, such a dynamic motion including a flight phase is still a challenging topic in humanoid robotics research, especially a running motion as shown in Fig. 1. This is not only because it is difficult to develop a humanoid mechanism and actuator capable of running, but also because the dynamics is constrained by the angular momentum (AM) conservation law in the flight phase. An error of the motion in the flight phase should be appropriately compensated because it directly affects the posture stability at the moment and after the touch down. Real-time control considering the AM conservation law is one of the important problems not only in the humanoid running control but also in the other robotics fields, such as space robotics and non-holonomic control [1], [2], [3], [4]. The knowledge for a floating-base system and AM control has been investigated also in humanoid robotics [5], [6]. Recently, we discussed the formulation of the AM Jacobian matrix and applied it to the resolved viscoelasicity control (RVC) in the previous report [7].

In recent years, the motion planning based on the whole-body dynamics has been an attracting research topic, solving a nonlinear optimization problem under the contact constraints [8], [9]. However, the computational cost of this approach is usually high. Therefore, more simplified models are often used for a real-time control. In the running motion, the trajectory of the center of gravity (COG) is important to obtain appropriate acceleration for take-off or touch-down. A lot of studies were investigated for the COG trajectory planning [10], [11], [12]. In particular, the spring-loaded inverted pendulum (SLIP) model is widely used [13], [14]

This research is supported by JSPS KAKENHI Grant Number 21H01282.
The authors are with the Department of Mechanical Engineering, Univ. of Tokyo, 7-3-1 Hongo, Bunkyo-ku, Tokyo 113-8656, Japan. he-zewen@ynl.t.u-tokyo.ac.jp

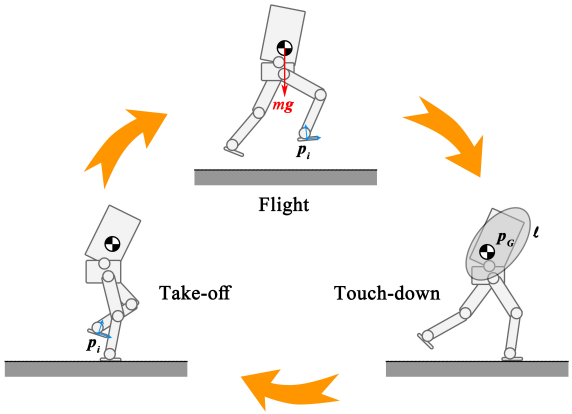


Fig. 1: Schematic diagram of humanoid robot running motion including three phases.

because it provides an intuitive physical dynamics for the acceleration for take-off and the deacceleration for the touch-down.

Compared to a walking motion, a difficulty in the running motion control is that we need to deal with a *non-linearity* even in a simple model. The famous linear inverted pendulum model [15] assuming that the COG height is constant cannot consider the acceleration of the COG height required for a running motion. The COG height acceleration makes the horizontal dynamics nonlinear. A lot of studies were proposed for dealing with this non-linearity, including nonlinear model predictive control, as summarized in [16]. Recently, a three-dimensional control of the zero moment point (ZMP) [17] was proposed [18], which can control the COG height acceleration by the *height* of the ZMP. This model was also applied to a running motion planning, allowing us to exclude the non-linearity in the simple COG-ZMP dynamics, even in a running motion. Based on this approach, we proposed a hopping strategy for humanoid push recovery [19].

In this paper, we present a running motion control by 1) the COG trajectory planning based on the 3D COG-ZMP model [18] and 2) the RVC method for the centroidal viscoelasicity [7] that we proposed in the previous report. Applying the centroidal RVC in the touch-down phase, we can improve the stability. We also present an on-line modification of the reference joint trajectory in the flight-phase, considering the AM conservation law. We validate the proposed running control through forward dynamics simulations.

The rest of the paper is organized as follows. In Section II, we overview the 3D COG-ZMP model of a humanoid robot.

Then, we explain the centroidal RVC method considering the AM dynamics in Section III, and present the on-line trajectory modification in Section IV. The results of forward dynamics simulations are reported in Section V. Finally, we summarize the obtained results in Section VI.

In the following sections, $\boldsymbol{E}$ and $\boldsymbol{O}$ denote identity and zero matrices, respectively. $\mathrm{diag}\{x_i\}$ denotes a diagonal matrix with the i-th diagonal element x_i. For a physical quantity $*$, $*_{ref}$ denotes the reference value, and $\Delta* := *_{ref} - *$ is the error from $*_{ref}$.

II. 3D COG-ZMP Model of a Humanoid [18]

The centoridal dynamics [6] of a humanoid robot is represented as follows:

$$\ddot{\boldsymbol{p}}_G = \frac{1}{m}\boldsymbol{f}_G - \boldsymbol{g} \tag{1}$$

$$\dot{\boldsymbol{\ell}} = \boldsymbol{n}_G \tag{2}$$

where $\boldsymbol{p}_G = [x_G\ y_G\ z_G]^T$ is the position of the center of gravity (COG), m is the total mass of the humanoid, $\boldsymbol{f}_G = [f_x\ f_y\ f_z]^T$ is the ground reaction force, $\boldsymbol{g} = [0\ 0\ g]^T$ is the gravity acceleration vector, $\boldsymbol{\ell}$ is the AM about the COG, and $\boldsymbol{n}_G$ is the total torque acting on the COG. We assume that the z-axis is along the vertical direction.

Equation (1) can be rewritten using the ZMP [17] as

$$\ddot{\boldsymbol{p}}_G = \omega^2(\boldsymbol{p}_G - \boldsymbol{p}_Z) - \boldsymbol{g} - \boldsymbol{S}\boldsymbol{n}_G, \tag{3}$$

$$\boldsymbol{S} := \frac{[\boldsymbol{\nu}\times]}{m\boldsymbol{\nu}^{\mathrm{T}}(\boldsymbol{p}_{\mathrm{G}} - \boldsymbol{p}_{\mathrm{Z}})} \tag{4}$$

where $\boldsymbol{p}_Z \in \mathbb{R}^3$ is the position of the ZMP. In this paper, we assume that the ZMP is defined on a plane that is vertical to the z-axis. In (4), the vector $\boldsymbol{\nu} = [0\ 0\ 1]^T$ is the unit direction vector of the z-axis. Also, ω in (3) is defined as follows:

$$\omega := \sqrt{\frac{\boldsymbol{\nu}^{\mathrm{T}}(\ddot{\boldsymbol{p}}_{\mathrm{G}} + \boldsymbol{g})}{\boldsymbol{\nu}^{\mathrm{T}}(\boldsymbol{p}_{\mathrm{G}} - \boldsymbol{p}_{\mathrm{Z}})}} = \sqrt{\frac{\ddot{z}_G + g}{z_G - z_Z}} \tag{5}$$

Usually, the value of ω changes as the vertical COG acceleration $\ddot{z}_G$ whereas z_Z is assumed to be constant. Then, controlling the ground reaction force in the z-axis is equivalent to controlling ω in the right-hand side of (3). From (3), we can extract the vertical ground reaction force as follows:

$$f_z = m\omega^2(z_G - z_Z) \tag{6}$$

Sugihara et al. [18] pointed that it is possible to generate equivalent ground reaction force changing z_Z with constant value of ω, which implies that the ZMP is defined as a three-dimensional control input. If we can consider a constant value of ω, (3) can be regarded as a linear time-invariant system, as described in the next section in detail.

In a humanoid system, we have the constraint on the ground reaction force: $f_z \geq 0$. From (6), this is equivalent to $z_Z \leq z_G$. The equality satisfies when a humanoid is in the flight state. From this property, Sugihara et al. [18] proposed an optimal-control-based method for generating the COG and ZMP trajectories of a running motion.

In this paper, we employ the same method for the running trajectory planning. The reference trajectory is obtained solving the inverse kinematics, especially considering the AM conservation law in the flight phase.

III. Touch-down Phase Control based on Resolved Centroidal Viscoelasticity [7]

A. Centroidal Feedback Control including Angular Momentum

The motion in the touch-down phase play an important role in a stable transition from the flight to take-off phases. In this paper, we employ the resolved centroidal viscoelasicity control in the touch-down phase, which was proposed in the previous report [7].

We transform (3) into a state equation to derive a feedback control to stabilize the COG state. We define the state variable $\boldsymbol{x}$ and the control input $\boldsymbol{u}$ as follows:

$$\boldsymbol{x} = \begin{bmatrix} \boldsymbol{p}_{\mathrm{G}} \\ \dot{\boldsymbol{p}}_{\mathrm{G}} \\ \boldsymbol{\ell} \end{bmatrix}, \quad \boldsymbol{u} = \begin{bmatrix} \boldsymbol{p}_Z \\ \boldsymbol{n}_G \end{bmatrix} \tag{7}$$

Then, we can rewrite (3) as

$$\dot{\boldsymbol{x}} = \boldsymbol{A}\boldsymbol{x} + \boldsymbol{B}\boldsymbol{u} + \boldsymbol{G}\boldsymbol{w} \tag{8}$$

$$\boldsymbol{A} = \begin{bmatrix} \boldsymbol{O} & \boldsymbol{E} & \boldsymbol{O} \\ \omega^2\boldsymbol{E} & \boldsymbol{O} & \boldsymbol{O} \\ \boldsymbol{O} & \boldsymbol{O} & \boldsymbol{O} \end{bmatrix}, \boldsymbol{B} = -\begin{bmatrix} \boldsymbol{O} & \boldsymbol{O} \\ \omega^2\boldsymbol{E} & \boldsymbol{S} \\ \boldsymbol{O} & \boldsymbol{E} \end{bmatrix}, \tag{9}$$

$$\boldsymbol{G} = \begin{bmatrix} \boldsymbol{O} & \boldsymbol{O} \\ \frac{1}{m} & \boldsymbol{O} \\ \boldsymbol{O} & \boldsymbol{E} \end{bmatrix} \tag{10}$$

where $\boldsymbol{w} \in \mathbb{R}^6$ is the external wrench applied to the COG, including the gravitational force.

Given the reference trajectories $\boldsymbol{x}_{ref}$ and $\boldsymbol{u}_{ref}$, the state feedback control law is given as follows:

$$\boldsymbol{u} = \boldsymbol{u}_{ref} + \boldsymbol{F}(\boldsymbol{x}_{ref} - \boldsymbol{x}) \tag{11}$$

where $\boldsymbol{F} \in \mathbb{R}^{6\times 9}$ is the state feedback gain matrix. In [7], $\boldsymbol{F}$ is given as follows:

$$\boldsymbol{F} = \begin{bmatrix} \mathrm{diag}\{\alpha_i\}\boldsymbol{E} & \frac{1}{\omega}\mathrm{diag}\{\alpha_i\}\boldsymbol{E} & \boldsymbol{O} \\ \mathrm{diag}\{\beta_i\}\boldsymbol{S}^\sharp & \frac{1}{\omega}\mathrm{diag}\{\beta_i\}\boldsymbol{S}^\sharp & \boldsymbol{D}_\ell \end{bmatrix} \tag{12}$$

where α_i and β_i $(i = 1, 2, 3)$ are gain parameters for the control inputs $\boldsymbol{p}_Z$ and $\boldsymbol{n}_G$, respectively, $\boldsymbol{D}_\ell$ is a damping coefficient for the AM, and $\boldsymbol{S}^\sharp$ is a pseudo-inverse matrix of $\boldsymbol{S}$. As in (4), $\boldsymbol{S}$ is a skew-symmetric matrix, and its physical meaning in (3) is that: 1) AM in x- and y- directions have the effect on COG in y- and x- directions, reversely; 2) AM in z-direction has no effect on COG. Thus, in the feedback gain, we should set the pseudo-inverse matrix $\boldsymbol{S}^\sharp$ (also a skew-symmetric matrix with null vector in the third row) to offset the effect of $\boldsymbol{S}$.

B. Resolved Centroidal Viscoelasticity

The feedback control (11) can be rewritten as follows [7]:

$$\begin{bmatrix} \boldsymbol{f}_G \\ \boldsymbol{n}_G \end{bmatrix} = \begin{bmatrix} \boldsymbol{f}_{G,ref} \\ \boldsymbol{n}_{G,ref} \end{bmatrix} + \mathcal{K}\Delta\boldsymbol{p}_G + \mathcal{D}\begin{bmatrix} \Delta\dot{\boldsymbol{p}}_G \\ \Delta\boldsymbol{\ell} \end{bmatrix} \tag{13}$$

where $\mathcal{K}$ and $\mathcal{D}$ are defined as

$$\mathcal{K} = \begin{bmatrix} -m\omega^2(\boldsymbol{E} + \mathrm{diag}\{\alpha_i\}) - m\boldsymbol{S}\mathrm{diag}\{\beta_i\}\boldsymbol{S}^\sharp \\ \mathrm{diag}\{\beta_i\}\boldsymbol{S}^\sharp \end{bmatrix}, \tag{14}$$

$$\mathcal{D} = \begin{bmatrix} -m\omega\mathrm{diag}\{\alpha_i\} - \frac{m}{\omega}\boldsymbol{S}\mathrm{diag}\{\beta_i\}\boldsymbol{S}^\sharp & -m\boldsymbol{S}\boldsymbol{D}_\ell \\ \frac{1}{\omega}\mathrm{diag}\{\beta_i\}\boldsymbol{S}^\sharp & \boldsymbol{D}_\ell \end{bmatrix} \tag{15}$$

See Appendix for the detailed derivation. Note that $\mathcal{K}$ is not square. This is because the integrated term does not exists for the AM $\boldsymbol{\ell}$.

We consider to achieve this feedback control by the following joint feedback control:

$$\boldsymbol{\tau} = \boldsymbol{\tau}_{\mathrm{ref}} + \boldsymbol{K}_\theta\Delta\boldsymbol{\theta} + \boldsymbol{D}_\theta\Delta\dot{\boldsymbol{\theta}}. \tag{16}$$

where $\boldsymbol{\tau}_{\mathrm{ref}}$ is the feed-forward torque calculated by the inverse dynamics, $\boldsymbol{K}_\theta$ and $\boldsymbol{D}_\theta$ are the joint space stiffness and viscosity matrices, respectively, and $\boldsymbol{\theta} \in \mathbb{R}^j$ is the joint angle vector.

From the observation of the virtual work principle presented in [7], the relationship between the centroidal and joint viscoelasticities is obtained as follows:

$$\mathcal{K}\boldsymbol{J}_G\boldsymbol{K}_\theta^{-1}\begin{bmatrix} \boldsymbol{J}_G^T & \boldsymbol{J}_{A*}^T \end{bmatrix} = \boldsymbol{E} \tag{17}$$

$$\begin{bmatrix} \boldsymbol{J}_G \\ \boldsymbol{J}_{AM} \end{bmatrix}\boldsymbol{D}_\theta^{-1}\begin{bmatrix} \boldsymbol{J}_G^T & \boldsymbol{J}_{A*}^T \end{bmatrix} = \mathcal{D}^{-1} \tag{18}$$

where $\boldsymbol{J}_G$ and $\boldsymbol{J}_{AM}$ are the COG and AM Jacobian matrices, respectively. $\boldsymbol{J}_{A*}$ is another AM Jacobian matrix that decouples the inertia term: mass and interita matrix of each link [7]. We omit the detailed equation of $\boldsymbol{J}_{A*}$ because of the page limitation.

Finally, we can obtain $\boldsymbol{K}_\theta$ and $\boldsymbol{D}_\theta$ solving the above two matrix equations. These two forms $\boldsymbol{AXB} = \boldsymbol{C}$ where $\boldsymbol{X}$ is $\boldsymbol{K}_\theta^{-1}$ or $\boldsymbol{D}_\theta^{-1}$. The general solution is given by $\boldsymbol{X} = \boldsymbol{A}^\sharp\boldsymbol{CB}^\sharp + (\boldsymbol{Y} - \boldsymbol{A}^\sharp\boldsymbol{AYBB}^\sharp)$ with arbitrary matrix $\boldsymbol{Y}$ [20].

IV. On-line Modification of Reference Trajectory in Flight Phase

In the flight phase of a running motion, the motion error at the beginning of the phase significantly affects the motion at the moment of touch-down, especially resulting in an error of the foot landing position.

In the floating-base system, the motion is constrained by the angular momentum coversation law, which is a non-holonomic constraint.

Let $\dot{\boldsymbol{q}} = \begin{bmatrix} \dot{\boldsymbol{q}}_0^T & \dot{\boldsymbol{\theta}}^T \end{bmatrix}^T$ denote the generalized velocity where $\dot{\boldsymbol{q}}_0$ and $\dot{\boldsymbol{\theta}}$ are the velocity twist of the base-link, and the joint angle velocity vector, respectively. In the flight phase, the relationship between $\dot{\boldsymbol{q}}$ and the COG velocity and AM is represented as follows:

$$\boldsymbol{\xi} := \begin{bmatrix} \dot{\boldsymbol{p}}_G \\ \boldsymbol{\ell} \end{bmatrix} = \mathcal{J}_C\dot{\boldsymbol{q}}, \quad \mathcal{J}_C := \begin{bmatrix} \mathcal{J}_G \\ \mathcal{J}_{AM} \end{bmatrix} \tag{19}$$

where $\mathcal{J}_G$ and $\mathcal{J}_{AM}$ are the COG and AM Jacobian matrices, respectively. These Jacobian matrices are for $\dot{\boldsymbol{q}}$ whereas $\boldsymbol{J}_G$ and $\boldsymbol{J}_{AM}$ in the previous section were for the joint velocity. The time derivative of $\boldsymbol{\xi}$ is calculated as follows:

$$\dot{\boldsymbol{\xi}} = \begin{bmatrix} \ddot{\boldsymbol{p}}_G \\ \dot{\boldsymbol{\ell}} \end{bmatrix} = -\begin{bmatrix} \boldsymbol{g} \\ \boldsymbol{0} \end{bmatrix} \tag{20}$$

The lower part of this equation represents the AM conservation law. For the simplicity, we consider the no-gravity situation and assume that $\boldsymbol{\xi}$ is constant. Considering the submatrices of the Jacobian matrix $\boldsymbol{J}_C$, we can rewrite (19) as follows:

$$\boldsymbol{\xi} = \underbrace{\begin{bmatrix} \boldsymbol{J}_{C0} & \boldsymbol{J}_{C\theta} \end{bmatrix}}_{\boldsymbol{J}_C}\begin{bmatrix} \dot{\boldsymbol{q}}_0 \\ \dot{\boldsymbol{\theta}} \end{bmatrix} = \boldsymbol{J}_{C0}\dot{\boldsymbol{q}}_0 + \boldsymbol{J}_{C\theta}\dot{\boldsymbol{\theta}} \tag{21}$$

Because $\boldsymbol{J}_{C0}$ is a regular matrix, we can calculate $\dot{\boldsymbol{q}}_0$ as follows:

$$\dot{\boldsymbol{q}}_0 = -{\boldsymbol{J}_{C0}}^{-1}\boldsymbol{J}_{C\theta}\dot{\boldsymbol{\theta}} + {\boldsymbol{J}_{C0}}^{-1}\boldsymbol{\xi} \tag{22}$$

We compensate the error of the landing foot position and attitude by the modification of the joint angle. Let $\dot{\boldsymbol{p}}_i$ and $\mathcal{J}_i$ denote the 6D velocity twist of the landing foot and its Jacobian matrix satisfying $\dot{\boldsymbol{p}}_i = \mathcal{J}_i\dot{\boldsymbol{q}}$, respectively. Using (22), this equation can be divided calculated as follows:

$$\dot{\boldsymbol{p}}_i = \mathcal{J}_i\begin{bmatrix} \dot{\boldsymbol{q}}_0 \\ \dot{\boldsymbol{\theta}} \end{bmatrix} = \boldsymbol{J}_i\dot{\boldsymbol{\theta}} + \boldsymbol{\zeta}_i, \tag{23}$$

$$\boldsymbol{J}_i := \mathcal{J}_i\begin{bmatrix} -{\boldsymbol{J}_{C0}}^{-1}\boldsymbol{J}_{C\theta} \\ \boldsymbol{E} \end{bmatrix}, \ \boldsymbol{\zeta}_i := \mathcal{J}_i\begin{bmatrix} {\boldsymbol{J}_{C0}}^{-1}\boldsymbol{\xi} \\ \boldsymbol{O} \end{bmatrix} \tag{24}$$

At each control cycle, the relationship between the error of the landing foot position and attitude $\Delta\boldsymbol{p}_i = \boldsymbol{p}_{i,ref} - \boldsymbol{p}_i$ and the corresponding joint angle is obtained as follows:

$$\Delta\boldsymbol{p}_i = \boldsymbol{J}_i\Delta\boldsymbol{\theta} + \Delta t\boldsymbol{\zeta}_i \tag{25}$$

where Δt is the sampling time. Note that in this paper we mainly focus on the compensation of the error in the x- and y- directions. It can be easily extended to the z-axis compensation explicitly considering the gravitational effect.

From the error $\Delta\boldsymbol{p}_i$ at each control cycle, we can calculate the compensation of the joint angle $\Delta\boldsymbol{\theta}$ solving (25). We can use the singularity-robust inverse [21] to avoid the numerical instability due to the singular posture. We add $\Delta\boldsymbol{\theta}$ to the original joint angle trajectory at each control cycle.

The method we proposed here is a kind of inverse kinematics considering the AM conservation law, which was applied in space robotics researches for floating-base system control [1], [4].

V. Running Motion Control Strategy and Simulation Results

A. Control Framework

Fig. 2 shows a diagram of the running motion control. The motion planner block calculates the referential trajectories of the COG, foot position and attitude, body attitude. Then it calculates the inverse kinematics and outputs the referential joint trajectory. It also calculates the inverse dynamics and

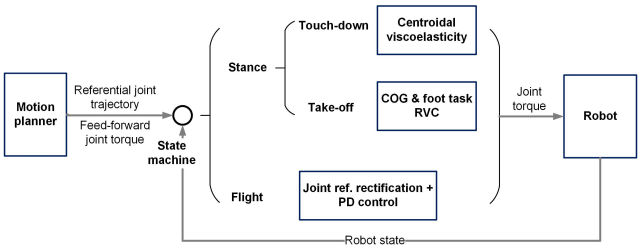


Fig. 2: Schematic diagram of control framework.

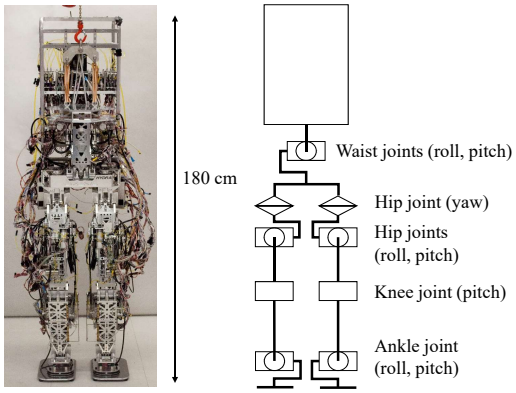


Fig. 3: External and joint configuration of Hydra.

outputs the feed-forward joint torque. A state machine detects which phase the robot belongs to, and selects the control method. The corresponding control methods are summarized as follows:

1) In the touch-down phase, we apply centroidal viscoelasticity control to stabilize the whole-body posture against the foot landing impact, whose main advantage is using the AM control to enlarge stabilizable region;
2) In the take-off phase, the COG and swing foot are controlled by the RVC method with high gains to achieve the referential COG acceleration with precise motion tracking at the lift-off moment;
3) In the flight phase, a simple joint PD control with high PD gains is applied, with the on-line modification of the reference trajectory mentioned in the previous section.

In a preliminary simulation, we found the foot landing impact caused a bounce of the foot on the ground. Therefore, we applied a "soft" PD control with low PD gains in a very short time (about 0.1s) at the beginning of the touch-down phase.

B. Simulation Environment and Setting

In this section, we validate the proposed method through forward dynamics simulations assuming a hydro-statically driven humanoid robot, Hydra (180cm, 74kg, 14 DOFs) as shown in Fig. 3 [22]. The motion generated by the method in Section II is a 9-step running (including 9 flight phases), with the double-support phase at the beginning and ending moment. Duration of every step is 0.7s, including 0.5s for stance phase and 0.2s for flight phase. Length of each step is 10cm. Inverse kinematics animation snapshots are shown in Fig. 4(a). In the simulation, we compare the following three cases:

1) Case 1: PD control in stance phase, without on-line modification in flight phase;
2) Case 2: PD control in stance phase, with on-line modification in flight phase;
3) Case 3: Proposed control method as in Fig. 2.

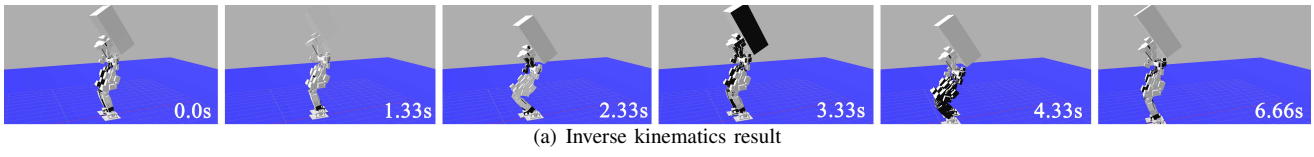
The setting of feedback gains are shown in the Table I. Note that PD gains at contact moment for impact mitigation are 300.0 (P) and 30.0 (D). Moreover, feed-forward torque generated by inverse dynamics is also applied during the whole stance phase.

C. Simulation Results and Discussion

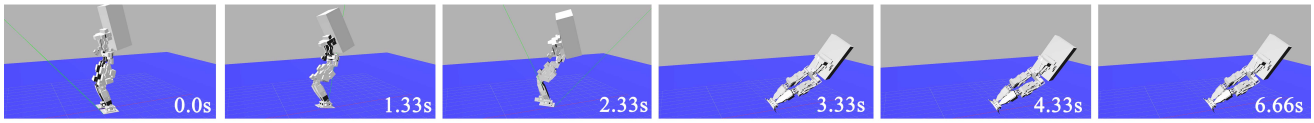
The animation snapshots of the simulated running motions are shown in Fig. 4 and the results of the COG and AM trajectories are in Figs. 5 and 6. In the simulation, only Case 3 achieved the running motion, tracking the reference COG trajectory accurately and controlling the AM in a limited range. Simple PD control in Case 1 and Case 2 did not achieve the running motion, and the robot fell over after the first step landing. From Fig. 5, it is observed that the COG was not precisely tracked to its reference in Case 1 and 2, especially in the x-direction. In Case 2, although the on-line modification was applied in the flight phase, the COG error of robot still occurred due to the PD control, so that the actual COG was far from the desired touch-down foot position, and then inverse kinematics cannot find a feasible solution. This situation can be found in the simulation video. In Case 3, on the other hand, the RVC with the centroidal viscoelasticity in the touch-down phase maintained the balance whereas the RVC with high feedback gain on the COG in the z-direction and swing foot task achieved an accurate tracking in the take-off phase. Furthermore, the on-line modification of the reference trajectory made the prospective touch-down of the foot landing contact with the ground. We consider that this is the reason why Case 3 achieved the running motion.

VI. Conclusion

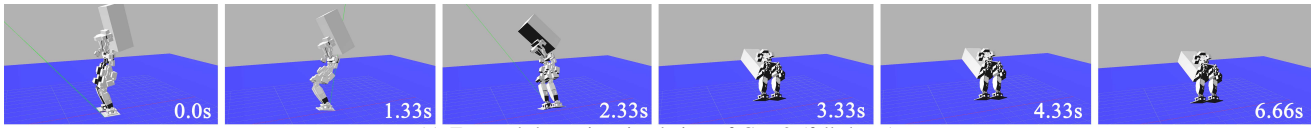
This paper presented a running motion control for a humanoid robot, consisting of the reference motion planning based on the 3D COG-ZMP model, the AM control in the touch-down phase by the centroidal RVC method, and the on-line trajectory modification in the flight phase. In the flight phase, we used the Jacobian matrix consdering the AM conservation law for compensating the error of the foot landing position and attitude. In the forward dynamics simulation, we achieved a 9-step running motion. The proposed method had a better performance than a simple PD control. Therefore, this result validates the feasibility and effectiveness of RVC, especially centroidal viscoelasticity control in the running motion.



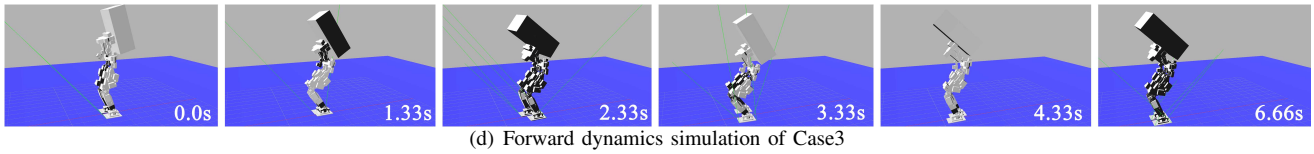
(a) Inverse kinematics result



(b) Forward dynamics simulation of Case1 (fall down)

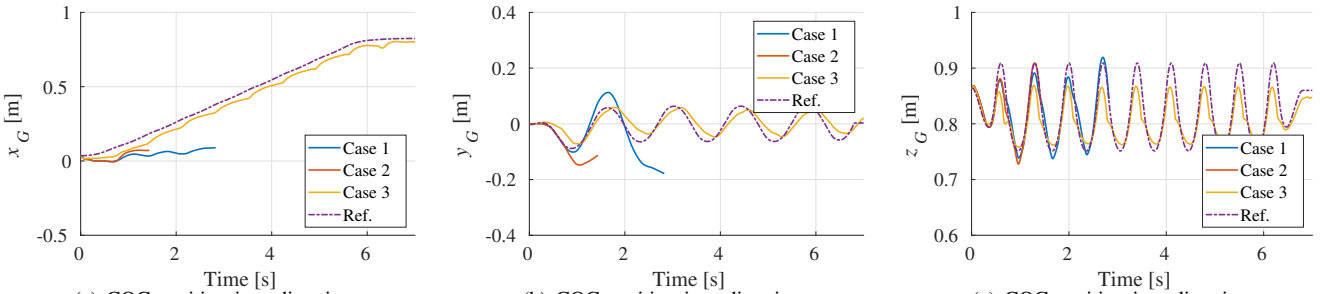


(c) Forward dynamics simulation of Case2 (fall down)



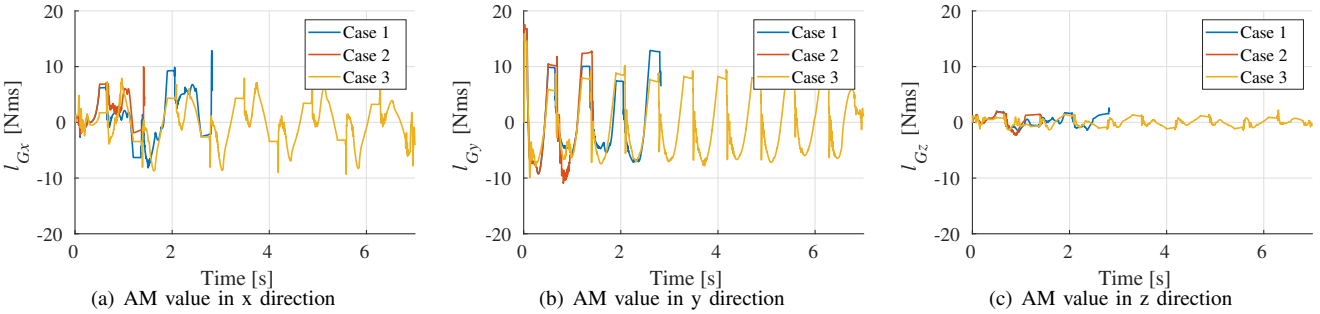
(d) Forward dynamics simulation of Case3

Fig. 4: Snapshots of running motion animation.



(a) COG position in x direction (b) COG position in y direction (c) COG position in z direction

Fig. 5: Simulation results of COG position in 3 directions. Blue, red and yellow lines represent COG of Case 1, Case 2 and Case 3, respectively, and purple dot-dash line is reference COG obtained by motion planner.



(a) AM value in x direction (b) AM value in y direction (c) AM value in z direction

Fig. 6: Simulation results of AM in 3 directions. Blue, red and yellow lines represent AM of Case 1, Case 2 and Case 3, respectively. The reference AM values in each direction and case are all zero.

TABLE I: Feedback gain setting in simulation

	Touch-down	Take-off	Flight
Joint PD for Case1 & Case2 and ref. viscoelasticity of Case3	P: 300.0 D: 30.0	P: 6000.0 D: 200.0	P: 2000.0 D: 200.0
Task feedback gain for Case3	COG (α_i): -2.0, -2.0, -200.0 AM (β_i): -2.0, -2.0, -2.0	COG (α_i): -2.0, -2.0, -1200.0 Foot pos.: P: 50000.0, D: 500.0 Foot att.: P: 5000.0, D: 20.0	(No task gain)

APPENDIX

DERIVATION OF (13) FROM (11) AND (12)

Substituting (12) into (11), we can obtain $\boldsymbol{p}_Z$ and $\boldsymbol{n}_G$ as follows:

$$\boldsymbol{p}_Z = \mathrm{diag}\{\alpha_i\}\Delta\boldsymbol{p}_G + \frac{1}{\omega}\mathrm{diag}\{\alpha_i\}\Delta\dot{\boldsymbol{p}}_G \tag{26}$$

$$\boldsymbol{n}_G = \mathrm{diag}\{\beta_i\}\boldsymbol{S}^{\#}\Delta\boldsymbol{p}_G + \frac{1}{\omega}\mathrm{diag}\{\beta_i\}\boldsymbol{S}^{\#}\Delta\dot{\boldsymbol{p}}_G + \boldsymbol{D}_\ell\Delta\boldsymbol{\ell} \tag{27}$$

From (3), $\boldsymbol{f}_G$ is calculated as follows:

$$\boldsymbol{f}_G = m\ddot{\boldsymbol{p}}_G = m\omega^2(\boldsymbol{p}_G - \boldsymbol{p}_Z) - m\boldsymbol{g} - m\boldsymbol{S}\boldsymbol{n}_G \tag{28}$$

Substituting (27) into (28) yields

$$\begin{aligned}\boldsymbol{f}_G = &-m\omega^2(\boldsymbol{E} + \mathrm{diag}\{\alpha_i\})\Delta\boldsymbol{p}_G - m\omega\mathrm{diag}\{\alpha_i\}\Delta\dot{\boldsymbol{p}}_G \\ &-m\boldsymbol{S}(\mathrm{diag}\{\beta_i\}\boldsymbol{S}^{\#}\Delta\boldsymbol{p}_G + \frac{1}{\omega}\mathrm{diag}\{\beta_i\}\boldsymbol{S}^{\#}\Delta\dot{\boldsymbol{p}}_G \\ &+\boldsymbol{D}_\ell\Delta\boldsymbol{\ell}) - m\boldsymbol{g}\end{aligned}$$

Thus, (13) is derived. Note that $\boldsymbol{S}\mathrm{diag}\{\beta_i\}\boldsymbol{S}^{\sharp}$ is calculated as

$$\boldsymbol{S}\mathrm{diag}\{\beta_i\}\boldsymbol{S}^{\sharp} = \begin{bmatrix}\beta_1 & 0 & 0\\ 0 & \beta_2 & 0\\ 0 & 0 & 0\end{bmatrix} \tag{29}$$

REFERENCES

[1] Y. Umetani, K. Yoshida, *et al.*, "Resolved motion rate control of space manipulators with generalized jacobian matrix," *IEEE Transactions on robotics and automation*, vol. 5, no. 3, pp. 303–314, 1989.

[2] Y. Nakamura and R. Mukherjee, "Nonholonomic Path Planning of Space Robots via a Bidirectional Approach," *IEEE Transactions on Robotics and Automation*, vol. 7, no. 4, pp. 500 – 514, 1991.

[3] Y. Nakamura, "Integrability of Dynamic Constraints of Underactuated Mechanisms," in *Proceedings of the 6th International Sympsium on Robotics Research*, 1993.

[4] D. N. Dimitrov and K. Yoshida, "Momentum distribution in a space manipulator for facilitating the post-impact control," in *2004 IEEE/RSJ international conference on intelligent robots and systems (IROS)(IEEE Cat. No. 04CH37566)*, vol. 4. IEEE, 2004, pp. 3345–3350.

[5] S. Kajita, F. Kanehiro, K. Kaneko, K. Fujiwara, K. Harada, K. Yokoi, and H. Hirukawa, "Resolved momentum control: humanoid motion planning based on the linear and angular momentum," in *Proceedings of IEEE/RSJ International Conference on Intelligent Robots and Systems*, vol. 2, 2003, pp. 1644–1650.

[6] D. E. Orin, A. Goswami, and S.-H. Lee, "Centroidal dynamics of a humanoid robot," *Autonomous Robots*, vol. 35, no. 2-3, pp. 161–176, 2013.

[7] Z. He and K. Yamamoto, "Decoupling of inertia effect in angular momentum of a humanoid and its application to resolved viscoelasticity control," in *2022 International Conference on Robotics and Automation (ICRA)*. IEEE, 2022, pp. 8490–8496.

[8] M. Posa, C. Cantu, and R. Tedrake, "A direct method for trajectory optimization of rigid bodies through contact," *The International Journal of Robotics Research*, vol. 33, no. 1, pp. 69–81, 2014.

[9] I. Mordatch, K. Lowrey, and E. Todorov, "Ensemble-cio: Full-body dynamic motion planning that transfers to physical humanoids," in *2015 IEEE/RSJ International Conference on Intelligent Robots and Systems (IROS)*. IEEE, 2015, pp. 5307–5314.

[10] T. Nagasaki, S. Kajita, K. Kaneko, K. Yokoi, and K. Tanie, "A running experiment of humanoid biped," in *2004 IEEE/RSJ International Conference on Intelligent Robots and Systems (IROS)(IEEE Cat. No. 04CH37566)*, vol. 1. IEEE, 2004, pp. 136–141.

[11] R. Tajima, D. Honda, and K. Suga, "Fast running experiments involving a humanoid robot," in *2009 IEEE international conference on robotics and automation*. IEEE, 2009, pp. 1571–1576.

[12] J. Englsberger, P. Kozłowski, C. Ott, and A. Albu-Schäffer, "Biologically inspired deadbeat control for running: from human analysis to humanoid control and back," *IEEE Transactions on Robotics*, vol. 32, no. 4, pp. 854–867, 2016.

[13] P. M. Wensing and D. E. Orin, "High-speed humanoid running through control with a 3d-slip model," in *2013 IEEE/RSJ International Conference on Intelligent Robots and Systems*. IEEE, 2013, pp. 5134–5140.

[14] A. Hereid, M. J. Powell, and A. D. Ames, "Embedding of slip dynamics on underactuated bipedal robots through multi-objective quadratic program based control," in *53rd IEEE Conference on Decision and Control*. IEEE, 2014, pp. 2950–2957.

[15] S. Kajita, F. Kanehiro, K. Kaneko, K. Fujiwara, K. Yokoi, and H. Hirukawa, "Biped walking pattern generation by a simple three-dimensional inverted pendulum model," *Advanced Robotics*, vol. 17, no. 2, pp. 131–147, jan 2003.

[16] K. Yamamoto, T. Kamioka, and T. Sugihara, "Survey on model-based biped motion control for humanoid robots," *Advanced Robotics*, vol. 34, no. 21-22, pp. 1353–1369, 2020.

[17] M. Vukobratović and J. Stepanenko, "On the stability of anthropomorphic systems," *Mathematical Biosciences*, vol. 15, pp. 1–37, 1972.

[18] T. Sugihara, K. Imanishi, T. Yamamoto, and S. Caron, "3d biped locomotion control including seamless transition between walking and running via 3d zmp manipulation," in *The 2021 IEEE International Conference on Robotics and Automation (ICRA)*. IEEE, 2021, pp. 6258–6263.

[19] K. Yamamoto, N. Kobayashi, T. Ishigaki, and Y. Sakemi, "Integration of Variable-height and Hopping Strategies for Humanoid Push Recovery (to be published)," in *Proceedings of IEEE Internatonal Conference on Intelligent Robots and Systems*, 2022.

[20] K. Yamamoto, "Robust walking by resolved viscoelasticity control explicitly considering structure-variability of a humanoid," in *2017 IEEE International Conference on Robotics and Automation (ICRA)*. IEEE, 2017, pp. 3461–3468.

[21] Y. Nakamura and H. Hanafusa, "Inverse kinematic solutions with singularity robustness for robot manipulator control," 1986.

[22] T. Ko, K. Murotani, K. Yamamoto, and Y. Nakamura, "Whole-body Compliant Motion by Sensor Integration of an Eha-Driven Humanoid Hydra," *International Journal of Humanoid Robotics*, vol. 2150002, pp. 1–26, 2021.